ACS APPLIED BIO MATERIALS

www.acsabm.org Article

Mechanistic Model for Drug Release from PLGA-Based Biodegradable Implants for *In Vitro* Release Testing: Development and Validation

Naresh Mittapelly,* Alexandre Djehizian, Krishna Chaitanya Telaprolu, Kevin McNally, Santosh Kumar Puttrevu, Omid Arjmandi-Tash, Sebastian Polak, and Frederic Y. Bois*

Cite This: https://doi.org/10.1021/acsabm.4c01054 Read Online

ACCESS | Metrics & More | Article Recommendations | Supporting Information

ABSTRACT: Several factors can affect drug release from polylactide coglycolide (PLGA)-based formulations, including polymer and drug properties, formulation components, manufacturing processes, and environmental *in vitro* or *in vivo* conditions. To achieve optimal release profiles for specific drug delivery applications, it is crucial to understand the mechanistic processes that determine drug release from PLGA-based formulations. In the current study, we developed a mechanistic model for the *in vitro* drug release of PLGA-based solid implants. The model accounts for all known critical quality attributes (CQAs) and considers the most important release rate processes, including water or dissolution medium influx into the porous structure of the implant, initial noncatalytic hydrolysis of PLGA, autocatalytic hydrolysis, dissolution of oligomers and monomers into the aqueous medium, the liberation of the trapped solid drug from the polymer matrix, dissolution of the solid drug into the wetted pore network, diffusion of the dissolved drug out of the implant, and distribution of the dissolved drug into the dissolution medium. The model has been validated using *in vitro* release data obtained from implants of four drugs (buserelin, afamelanotide, brimonidine, and nafarelin). The model presented in this manuscript provides valuable insights into the kinetics and mechanism of drug release from PLGA-based solid implants and has demonstrated the potential for optimizing formulation design. The *in vitro* release model, coupled with physiologically based pharmacokinetic (PBPK) modeling, can predict the *in vivo* performance of implants and can be used to support bioequivalence studies in a drug development program.

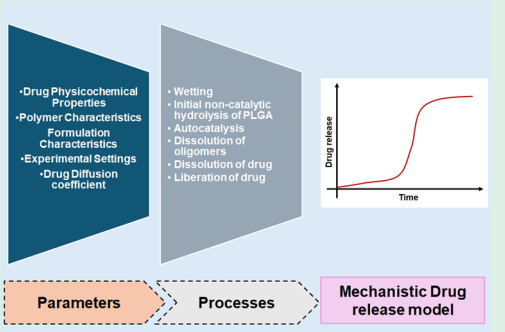

KEYWORDS: *long-acting injectables, biodegradable implants, PLGA-based solid implants, in vitro release testing, mechanistic modeling*

1. INTRODUCTION

Poly(lactide-*co*-glycolide) (PLGA)-based formulations were first approved for clinical use by the U.S. Food and Drug Administration (FDA) in 1989 in the case of Lupron Depot.[1] Since then, the FDA has approved 24 other innovator drug products using PLGA as the main excipient to achieve sustained release.[2] PLGA-based formulations offer a therapeutic advantage in the treatment of diseases requiring long durations of drug exposure with sustained levels of therapeutic concentrations.[3−8] PLGA is biodegradable and biocompatible, so PLGA-based drug products were approved for parenteral use by regulatory authorities. Biodegradation of PLGA is driven by an initial water influx followed by pH-driven rate-controlled degradation (ester hydrolysis) into short-chain oligomers. Further degradation of oligomers results in the formation of free acid molecules, resulting in a further drop in the pH, which further increases the hydrolysis rate. This phenomenon is termed autocatalytic degradation. The time-dependent degradation of polymers results in an increase in the porosity of the polymeric matrix, leading to drug release. Consequently, PLGA formulations offer rate-controlled drug release predominantly by diffusion through the water-filled porous structure of the polymeric matrix, osmotic pumping, and erosion.[9] Drug release from PLGA polymers typically lasts from days to months.

Fredenberg et al.[9] and Park et al.[10] discussed that drug release from PLGA-based formulations is influenced by several physicochemical properties of the polymer (molecular weight, lactic acid (LA) to glycolic acid (GA) ratio, acid or ester end-capping, crystallinity), drug (chemical properties, drug loading, content uniformity), drug delivery system (size, porosity, density, and shape), *in vitro* (release medium composition, pH, temperature, stirring rate, osmolality), and *in vivo* conditions (immune response, sink conditions, enzymes, lipids).

Received: July 29, 2024
Revised: October 9, 2024
Accepted: October 11, 2024

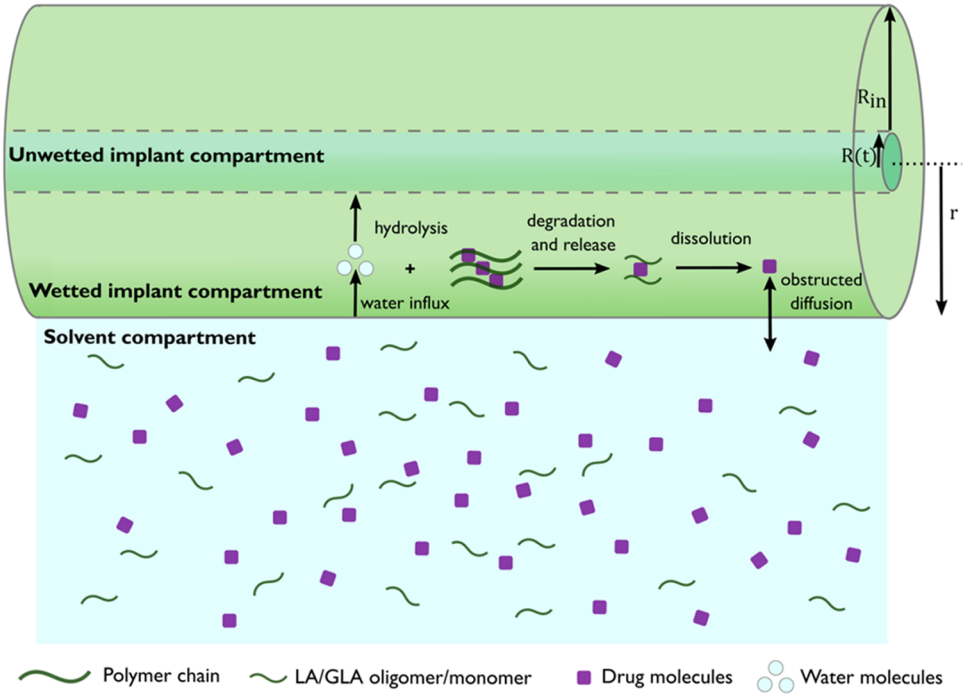

Figure 1. Schematic of the mechanistic release model, where arrows indicate physical or chemical processes. The schematic shows three regions: unwetted, wetted, and solvent/dissolution media compartments. $R(t)$ demarcates the boundary between unwetted and wetted compartments, and R_{im} indicates the radius of the implant.

Drug release is influenced not only by the physicochemical properties of the polymer and drug but also by the processes employed in manufacturing.[9,10] For example, the hot melt extrusion method leads to less porous implants compared to implants produced by direct compression.[11] Critical process parameters (CPPs) such as extrusion temperature, screw speed and feed rate, cooling rate, and melt viscosity for hot melt extrusion can have an impact on critical quality attributes (CQAs) of PLGA implants such as its porosity and, therefore, drug release.

Although PLGA-based injectable formulations offer several therapeutic advantages, their development is challenging, which is evident from their limited availability on the market. As described by Park et al.[10] and Yun et al.,[12] the bioavailability of API released from long-acting injectable (LAI) dosage forms, unlike the one released from oral dosage forms, cannot be predicted simply by drug properties because the release is predominantly influenced by the implant properties, polymer characteristics, and implant type. Drug release from most of the marketed PLGA drug delivery systems is characterized by an initial burst release followed by a slow drug release phase and is influenced by drug loading.[10,12] A high drug loading, with a low burst, is intended from a dosage form design perspective, the large pores in solid implants; however, a high drug loading can cause the burst release to occur initially, which is why it is important to maintain a balance between burst release and drug loading during development.[13,14] Additionally, the sensitivity of drug release toward the *in vitro* media testing conditions is also difficult to control.[13]

The implementation of the Quality by Design (QbD) approach ensures the development of quality drug products throughout their life cycle and helps overcome the challenges associated with their development. In summary, the QbD approach involves Quality Target Product Profile (QTPP) construction, which can be achieved by controlling CQAs and CPPs. Mechanistic mathematical models are one of the key elements of the QbD approach.[15] Furthermore, *in vitro* release testing (IVRT) is a useful technique for evaluating product performance and is widely reported to be used for understanding product behavior when changing formulation factors or manufacturing conditions. Unfortunately, IVRT alone does not provide quantitative insights into the release behavior of new or alternative formulations manufactured. Mathematical modeling is a tool to bridge the gap between the generated information from IVRT and the CQAs of the product. By using mathematical models to understand the underlying mechanisms of drug release, researchers can predict the release kinetics of drugs from PLGA implants and make informed decisions about the design and optimization of the delivery system. The use of mathematical models can help to reduce the number of physical experiments that are needed to determine the optimal design of the delivery system. Consequently, this approach can potentially save time and resources during the initial drug product development phase for new chemical entities (NCEs) and generic equivalents.

Mathematical modeling of drug release from PLGA formulations was extensively reviewed in the literature.[16] Most of the published mathematical models emphasize one of the processes involved in drug release, either PLGA degradation,[17−21] erosion with pore formation, diffusive drug release, stochastic degradation and erosion, erosion by dissolution to determine microclimate pH, noncatalytic and autocatalytic degradation,[22−26] or show empirical fits between drug diffusivity and degradation.[27−30] A few models interlinking different phenomena of drug release from PLGA formulations were also reported.[31−41] However, these coupled phenomena models do not account for all of the key processes involved in drug release from the PLGA matrices. Furthermore, most of the mathematical models were developed for microspheres, and a comprehensive mechanistic model of drug release from PLGA-

https://doi.org/10.1021/acsabm.4c01054
ACS Appl. Bio Mater. XXXX, XXX, XXX−XXX

based implants is still lacking. Therefore, the present study aims to address the gaps in existing models by developing a comprehensive mathematical model to predict the *in vitro* drug release from solid implants by accounting for the CQAs of these formulations. Attention has been paid toward the inclusion of drug, polymer, and formulation-related parameters in the model, and in most cases, they can be either measured or predicted (*i.e.*, calculated). The model has been validated with *in vitro* release data obtained from implants with four different compounds to demonstrate its applicability and performance.

2. MATERIALS AND METHODS

We developed a predictive, bottom-up, mechanistic model that encapsulates all of the following underlying rate processes leading to the drug release from PLGA-based solid implant formulations:

1. Water/dissolution media influx into the porous structure of the implant.
2. Initial noncatalytic hydrolysis of PLGA while the concentration of acid end groups on the polymer chains is low.
3. Autocatalytic hydrolysis phase when the catalyst concentration is pronounced.
4. Dissolution of small oligomers and monomers into the aqueous medium characterized by substantial mass loss of the polymer and the growing pore network.
5. Liberation of the trapped solid drug from the formulation PLGA polymer matrix.
6. Dissolution of solid drugs into the wetted pore network.
7. Diffusion of the dissolved drug out of the implant through pores.
8. Accumulation of the dissolved drug in the dissolution media.

The developed model, along with the above-mentioned rate processes, is illustrated schematically in Figure 1 and should be understood to be spatially structured, as indicated therein by three compartments: unwetted implant compartment, wetted implant compartment, and solvent compartment. A detailed description of the rate processes and their governing equations in each compartment can be found in the following section. Further, to evaluate model performance, we used fold error (simulated-to-observed data ratio) as a metric; a ratio within the range of 0.5−2 is considered acceptable.

2.1. Modeling of Drug Release from PLGA Implants.

2.1.1. Water/Dissolution Media Influx. Recent investigations of the microstructure characterization of long-acting polymeric implants revealed a clear wetted front (and thus a release front) inside the implant during the *in vitro* release experiments. This wetted front advances radially from the outer edge of the cylindrical implant toward its central axis during the release experiments and divides the implant into the wetted and unwetted regions, as shown in Figure 1. The kinetics of the wetting and liquid penetration inside the porous implant depends on the microstructural characteristics of the implant such as porosity and pore size, and the penetrating liquid properties, such as its viscosity. Our aim in this section is to develop a mechanistic model that can predict the wetting kinetics of the dissolution media inside the PLGA implant as a function of both liquid and implant properties.

The kinetics of water/dissolution media penetration in a porous medium such as a PLGA implant, in the radial direction can be described by Darcy's equation:

$$\frac{1}{r}\frac{\partial}{\partial r}(rv) = 0,\ v = \frac{\kappa_p}{\mu}\left|\frac{\partial p}{\partial r}\right| \tag{1}$$

where v is the flux (radial velocity) of the liquid inside the porous medium, κ_p is the permeability of the porous medium, μ is the viscosity of the dissolution media, and $\frac{\partial p}{\partial r}$ is the pressure gradient in the radial direction causing the liquid influx. Equation 1 assumes that the rate of increase of solid matrix volume is equal to the volumetric rate of liquid absorption by the solid matrix. The solution of the latter equations is

$$p = -\left(\frac{c\mu}{\kappa_p}\right)\ln(r) + b;\ v = \frac{c}{r} \tag{2}$$

where b and c are integration constants, which should be determined using the boundary conditions for the pressure at the implant edge, where $r = R_{im}$ (implant radius), and at the circular edge of the wetted region inside the porous implant, where $r = R(t)$, with $R(t)$ being the radius of the circular edge of the wetted region of the implant.

The boundary condition at the edge of the implant is

$$p = p_r \text{ at } r = R_{im} \tag{3}$$

The boundary condition at the circular edge of the wetted region inside the porous implant is

$$p = p_r - p_{im} \text{ at } r = R(t) \tag{4}$$

where p_r is an unknown reference pressure within the tissue, $p_{im} \approx \frac{2\gamma\cos\theta}{R_p}$ is the capillary pressure inside the pores of the implant, γ is the surface tension of the dissolution media, θ is the contact angle or hydrophobicity of the implant, and R_p is a characteristic scale of the pore radius inside the implant.

Taking into account the latter two boundaries, both integration constants, b and c, can be determined, which gives the following expression for the radial velocity (flux) of dissolution media:[42]

$$v = \frac{\kappa_p}{\mu}\frac{p_{im}}{R(t)\times\ln\left(\frac{R(t)}{R_{im}}\right)} \tag{5}$$

The velocity at the circular edge of the wetted region inside the implant is

$$\varepsilon_{SF}\frac{dR(t)}{dt} = v|_{r=R(t)} \tag{6}$$

where ε_{SF} is the porosity of the implant. A combination of the latter two equations gives the evolution equation for $R(t)$:

$$\frac{dR(t)}{dt} = \frac{\kappa_p}{\varepsilon_{SF}\mu}\frac{p_{im}}{R(t)\times\ln\left(\frac{R(t)}{R_{im}}\right)} \tag{7}$$

And therefore, the volume of the absorbed liquid inside the implant can be found by

$$W(t) = \varepsilon_{SF}(t)L_{im}\pi[R_{im}^2 - R(t)^2] = \varepsilon_{SF}(t)V_{im}\left(1 - \frac{R(t)^2}{R_{im}^2}\right) \tag{8}$$

where L_{im} and V_{im} are the length and volume of the implant, respectively.

If we adopt the Kozeny−Carman model of the porous medium[43] considering the pore space as a packed bed, the permeability can be approximated by

$$\kappa_p = D_w\frac{\varepsilon_{SF}^3}{(1-\varepsilon_{SF})^2}\frac{(2R_p)^2}{180} \tag{9}$$

where D_w is a permeation scalar used to recover the observed data, as required.

2.1.2. PLGA Degradation. Since the trapped drug is released during the degradation of the implant, it is important to begin with the degradation dynamics of PLGA. The hydrolysis and degradation of PLGA occur through two spatially separable processes known as surface- and bulk-hydrolysis. The liquid/water in contact with the PLGA solid surface initiates hydrolysis and degradation. The kinetics of liquid penetration in a porous PLGA implant are discussed and predicted in the previous section based on a modified Darcy's equation and the wettability of the implant. Accordingly, the degradation and hydrolysis of a highly wettable implant mainly occur from the bulk of the implant, where most of the surface-accessible pores are occupied by the penetrating liquid. In this case, hydrolysis is taking place within the

https://doi.org/10.1021/acsabm.4c01054
ACS Appl. Bio Mater. XXXX, XXX, XXX−XXX

liquid-saturated pores inside the implant, and the degradation proceeds through bulk-hydrolysis (bulk erosion). In contrast, for less wettable or nonwettable implants, degradation mainly occurs from the surface of the implant, as it is mainly controlled by surface hydrolysis (surface erosion).

To develop a kinetic model for PLGA degradation, we begin with the hydrolysis and depolymerization reaction kinetics in the presence of water. Experimental data suggest that this hydrolysis reaction is catalyzed by an acid (H^+ ions). We assume that polymers can be of different types (indexed by i), depending on their composition (see Figure 2). The fraction in moles (molar ratio) of polylactic acid (PLA,

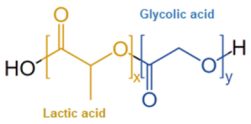

Figure 2. Structure of poly(lactic-*co*-glycolic acid); x = number of units of lactic acid; y = number of units of glycolic acid. The localization of the various monomers can be more or less random.

type 1) polymers in the PLGA polymer mixture is ψ, and it is known from the manufacturing process. For a polymer of the type i and any given chain of j monomers, the net hydrolysis reaction can be summarized by

$$P_{i,j} + H_2O + H^+ \rightarrow P_{i,m} + P_{i,j-m} + H^+,\ j = 2, 3, ..., L_p \text{ and } m = 1, 2, ..., j-1$$

where i = 1 and 2 correspond to polylactic acid (PLA) and polyglycolic acid (PGA), respectively, and L_p is the initial chain length. This degradation process is schematically shown in Figure 3.

To handle the complex process of long-chain polymer degradation, we derived a similar but more sophisticated relation,[44] describing the probabilistic degradation of a polymer chain length distribution. For any given chain of j monomers, the number of hydrolytically accessible bonds is $(j-1)$. The rate of hydrolysis of PLGA polymers of a given size can be assumed to be proportional to the number of hydrolytically accessible bounds it contains $(j-1)$, to a hydrolysis rate per bond ($K_{hyd,i}$), to the concentration of H^+ ions in the volume where the reaction is taking place, and to the mass of the polymer present in the reaction volume. A full description of the hydrolysis reaction would model the binding of H^+ to PLGA, the subsequent breakage of the chain into two smaller polymers, and the release of H^+. The fact is that the availability of H^+ is rate limiting and that there is competition between the various polymer bonds in binding H^+. To take this competition into account, we assume that the probability for polymers of size j to bind H^+ is equal to the total number of bounds they contain ($j-1$ bonds times the number of polymer molecules of size j) divided by the total number of bounds present in the reaction volume. For nondissolved (p) and dissolved (q) polymers, the corresponding probabilities are therefore (eqs 10 and 11):

$$\mathbb{P}_{p_{i,j}}(p_{i,j} \text{ is hydrolyzed}) = \frac{\frac{(j-1)p_{i,j}(t)}{j \times Mw_{M_i}}}{\sum_{i=1}^{2}\left[\left(\sum_{j=2}^{J_{i,\min}-1}\frac{(j-1)q_{i,j}(t)}{j \times Mw_{M_i}}\right)+\left(\sum_{j=J_{i,\min}}^{L_p}\frac{(j-1)p_{i,j}(t)}{j \times Mw_{M_i}}\right)\right]} \quad (10)$$

$$\mathbb{P}_{q_{i,j}}(q_{i,j} \text{ is hydrolyzed}) = \frac{\frac{(j-1)q_{i,j}(t)}{j \times Mw_{M_i}}}{\sum_{i=1}^{2}\left[\left(\sum_{j=2}^{J_{i,\min}-1}\frac{(j-1)q_{i,j}(t)}{j \times Mw_{M_i}}\right)+\left(\sum_{j=J_{i,\min}}^{L_p}\frac{(j-1)p_{i,j}(t)}{j \times Mw_{M_i}}\right)\right]} \quad (11)$$

where $J_{i,\min}$ is the oligomers' chain length below which they are considered to be dissolved and capable of diffusing within the liquid-occupied pores inside the implant ($J_{i,\min} \approx 16$) experimentally determined by size exclusion chromatography.[45] Note that the masses here should be molar or, equivalently, numbers of molecules in the reaction volume (the individual i monomers have the molecular weight Mw_{M_i}).

Given the above considerations, we derive eq 12 to track the mass of nondissolved polymers with specific chain lengths for lactide (LA) and glycolide (GA) oligomers, $p_{i,j}(t,r)$, over the reaction time and along the radius of the implant.

$$\frac{\partial}{\partial t}\frac{p_{i,j}(t,r)}{j \times Mw_{M_i}} = K_{hyd,i}\cdot[H^+](t,r)\left[\left(\sum_{k=j+1}^{L_p}\mathbb{P}_{p_{i,k}}\frac{2}{k-1}\frac{p_{i,k}(t,r)}{k \times Mw_{M_i}}\right) - \mathbb{P}_{p_{i,j}}\frac{p_{i,j}(t,r)}{j \times Mw_{M_i}}\right] \quad \text{with } j \geq J_{i,\min},\ r \in [R(t), R_{im}) \quad (12)$$

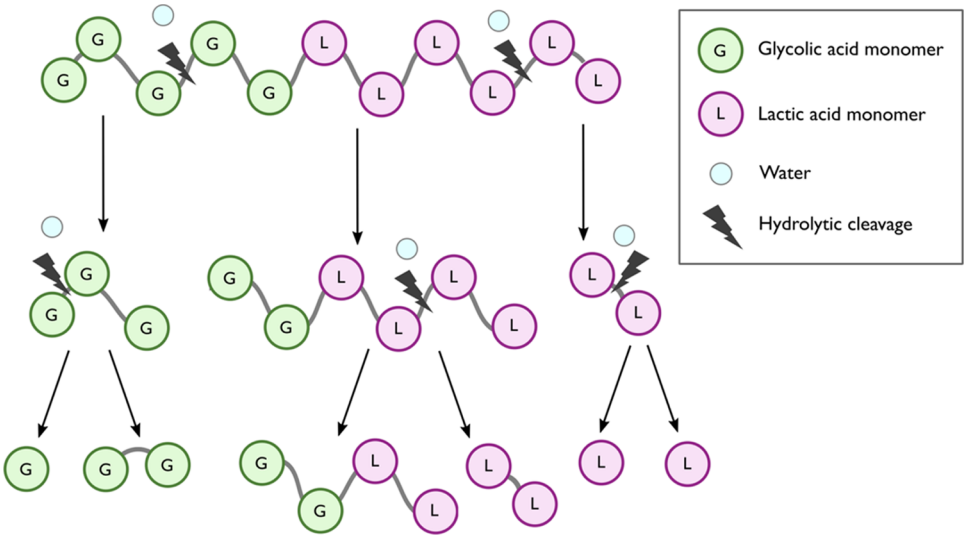

Figure 3. Schematic of PLGA polymer degradation in the presence of water molecules.

https://doi.org/10.1021/acsabm.4c01054
ACS Appl. Bio Mater. XXXX, XXX, XXX−XXX

The radial hydrogen ion distribution over the reaction time, $H^+(t,r)$, is described in Section 2.1.5. Accordingly, the mass of dissolved polymers, $q_{i,j}(t,r)$, and time evolution along the implant radius can be described by the following eq (eq 13):

$$\frac{\partial}{\partial t}\frac{q_{i,j}(t,r)}{j \times Mw_{M_i}} = -\omega_{q,m}(t)\frac{D_{d,if}}{r}\frac{\partial}{\partial r}\left(r\frac{\partial}{\partial r}\frac{q_{i,j}(t,r)}{j \times Mw_{M_i}}\right) + K_{hyd,i}\cdot[H^+](t,r)\left[\sum_{k=j+1}^{J_{i,min}-1}\left(\mathbb{P}_{q_{i,k}}\frac{2}{k-1}\frac{q_{i,k}(t,r)}{k \times Mw_{M_i}}\right) + \sum_{k=J_{i,min}}^{L_p}\left(\mathbb{P}_{p_{i,k}}\frac{2}{k-1}\frac{p_{i,k}(t,r)}{k \times Mw_{M_i}}\right) - \mathbb{P}_{q_{i,j}}\frac{q_{i,j}(t,r)}{j \times Mw_{M_i}}\right]$$

$$\text{with } j < J_{i,min},\ r \in [R(t),\ R_{im}) \tag{13}$$

The first term on the right-hand side of the above equation accounts for the obstructive diffusion of the dissolved polymer molecules through the pore network radially from the center to the surface of the implant. It depends on the obstruction coefficient for the diffusive species $\omega_{q,m}(t)$ (see Section 2.1.6). $D_{q,if}$ is the diffusivity of dissolved polymers in the dissolution media, assumed to be the same for oligomers with different chain lengths. The second term accounts first for the hydrolysis of dissolved polymers yielding polymer $q_{i,j}$, next for the hydrolysis of undissolved polymers yielding $q_{i,j}$, and finally, the hydrolysis of $q_{i,j}$ itself.

2.1.3. Liberation of the API from the PLGA Polymer Matrix. We assume that a fraction of the drug is trapped in the polymer matrix and is not immediately available for dissolution into the wetted pores. This trapped fraction of the drug is released and should come in contact with water at the surface of the pores as the nondissolved polymer is hydrolytically degraded in the wetted portion of the implant. Therefore, we assume that the release rate of the trapped drug is proportional to the nondissolved polymer degradation rate,[7] as described by the following equation:

$$\frac{\partial}{\partial t}\xi(t,r) = \frac{\xi(t=0,r)}{\sum_{i=1}^{2}\sum_{j=J_{i,min}}^{L_p} p_{i,j}(t=0,r)}\cdot\frac{\partial}{\partial t}\sum_{i=1}^{2}\sum_{j=J_{i,min}}^{L_p} p_{i,j}(t,r)$$

$$r \in [R(t),\ R_{im}) \tag{14}$$

where $\xi(t,r)$ is the mass of the trapped solid drug. As the polymer degradation proceeds, the drug is moved from a trap to an untrapped state, and it becomes available for subsequent dissolution into the wetted pore network, as described in the following section.

2.1.4. Dissolution and Distribution of the API. Dissolution of the untrapped API from the PLGA polymer matrix is handled by a modified diffusion layer model (DLM). The DLM model itself is used by the Simcyp simulator, and it is based on the Wang Flanagan model.[46] Diffusion layer models, sometimes called thin-film models, assume that there is a hydrodynamic boundary layer of effective thickness, h_{DLM}, surrounding the solid drug particles and that diffusion of dissolved drug through this layer into bulk solution is the rate-limiting step of the dissolution process. DLMs originated with the work of Noyes–Whitney[47] later extended by Nernst[48] and Brunner.[49] These models assume a linear decrease in the concentration of the dissolving compound when moving from the solid surface to the hydrodynamic boundary layer limit. Noyes and Whitney models consider dissolution from a planar surface, while the Wang and Flanagan model was derived for spherical geometry and applies for dissolution from spherical particles.

The modified DLM for the dissolution of the API from the PLGA polymer matrix considers both the release of API from the polymer matrix due to degradation (as described in the previous section) and the dissolution of the released API from the pore surfaces into the bulk solution inside the wetted pores (Figure 4).

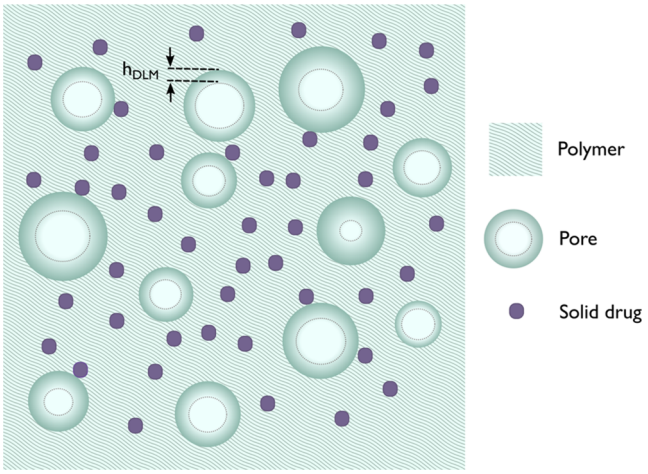

Figure 4. Illustration of the modified DLM model for release and dissolution of API: A fraction of pore surfaces is covered by solid drug, and dissolution happens from those parts of the pore surfaces covered by solid drug (untrapped drug). The rate-limiting step for the dissolution of this untrapped drug is the diffusion within the effective thickness, h_{DLM}.

In this case, we assume that the surface of the pores is partially covered with solid drug (i.e., untrapped drug) and the rate-limiting step for the dissolution of this untrapped drug is the diffusion within the effective thickness h_{DLM} (as shown in Figure 4), from the pore surfaces into the bulk solution inside the pores (eq 15):

$$\frac{\partial}{\partial t}m(t,r) = -\sigma_\Lambda\cdot SA_p(t,r)\frac{D_{c,if}}{h_{DLM}}(C_s(t,r) - C(t,r)) - \frac{\partial}{\partial t}\xi(t,r)$$

$$r \in [R(t),\ R_{im}) \tag{15}$$

where m is the mass of the released solid drug (from the polymer matrix after its degradation), available for dissolution, $D_{C,if}$ is the drug diffusivity in the dissolution media, $SA_p(t,r)$ is the surface area of the pores (eq 22), σ_Λ is the surface fraction of the pores which are covered with solid drug (assumed to be equal to the fractional mass loading of drug in the implant: dose divided by the initial mass of the implant, M_{im}), C_s is the aqueous (or dissolution medium) solubility of the drug (pH dependent obtained by Henderson–Hasselbalch equations for different compound types depending on their dissociation constants, pK_a1 and pK_a2), h_{DLM} is the diffusion layer thickness (by default considered to be equal to the average pore radius, R_p), and C is the concentration of dissolved drug within the pores of an implant, which can be obtained by (eq 16):

$$\frac{\partial}{\partial t}C(t,r) = -\omega_{c,m}(t)\frac{D_{C,if}}{r}\frac{\partial}{\partial r}\left(r\frac{\partial}{\partial r}C(t,r)\right) + \sigma_\Lambda\cdot\frac{SA_p(t,r)}{V_p(t,r)}\frac{D_{C,if}}{h_{DLM}}(C_s(t,r) - C(t,r))$$

$$r \in [R(t),\ R_{im}) \tag{16}$$

The first term on the right-hand side of the above equation accounts for the obstructive diffusion of the dissolved drug molecules through the pore network radially from the center to the surface of the implant. The second term corresponds to the dissolution of the untrapped drug. $SA_p(t,r)/V_p(t,r)$ can be approximated by $2/R_p(t)$ in the above equation.

https://doi.org/10.1021/acsabm.4c01054
ACS Appl. Bio Mater. XXXX, XXX, XXX−XXX

After release, dissolution, and diffusion through the pore network, the drug molecules reach the solvent compartment and accumulate there over the time course of the *in vitro* release testing experiment.

Accordingly, the concentration of the drug in the peri-implant solvent compartment, $C_{if}(t,r)$, can be obtained by (eq 17):

$$\frac{\partial}{\partial t}C_{if}(t,r) = -\frac{D_{C,if}}{r}\frac{\partial}{\partial r}\left(r\frac{\partial}{\partial r}C_{if}(t,r)\right)$$
$$r \in [R_{im}, \infty) \tag{17}$$

2.1.5. Dynamics of H^+ Ionization and Distribution. During the polymer hydrolysis process, the acidic polymer fragments and byproducts accumulate inside the interior of the implant and further catalyze the hydrolysis reaction. This autocatalytic effect accelerates the reaction time and eventually leads to a secondary burst phase in the release profile of the drug. The dynamics of ionization due to dissociation equilibrium for polymeric species with acid groups and radial H^+ distribution within the implant ($H^+(t,r)$) and in the peri-implant solvent compartment ($H_{if}^+(t,r)$) are described by (eqs 18 and 19):

$$\frac{\partial}{\partial t}H^+(t,r) = -\omega_{H^+,m}(t)\frac{D_{H^+,if}}{r}\frac{\partial}{\partial r}\left(r\frac{\partial}{\partial r}H^+(t,r)\right) + k_p^+[H^+]\sum_{i=1}^{N_p}\left(K_{hyd,i}\sum_{j=J_{i,min}}^{L_p}\frac{p_{i,j}(t,r)}{j \times Mw_{M_i}} + \sum_{j=1}^{J_{i,min}-1}\frac{q_{i,j}(t,r)}{j \times Mw_{M_i}}\right) - \frac{k_p^-}{V_{intra}(t)}H^{+2}(t,r)$$
$$r \in [R(t), R_{im}) \tag{18}$$

$$\frac{\partial}{\partial t}H_{if}^+(t,r) = -\frac{D_{H^+,if}}{r}\frac{\partial}{\partial r}\left(r\frac{\partial}{\partial r}H_{if}^+(t,r)\right)$$
$$r \in [R_{im}, \infty) \tag{19}$$

where, $D_{H^+,if}$ is the diffusivity of the H^+ ions, $\omega_{H^+,m}$ is the obstruction coefficient for the diffusion of H^+ ions through the pore network, and k_p^+ and k_p^- are the polymer ionization and deionization proportionality and rate constants, respectively. Note that in both equations, unknowns H^+ and H_{if}^+ are in mol to avoid handling concentrations with a time-changing volume of fluid $V_{intra}(t)$, which would lead to an additional term in the equations. The brackets around H^+ represent its (molar) concentration.

2.1.6. Auxiliary Equations. Degradation, erosion, and dissolution of oligomers and monomers and subsequent release and dissolution of drug particles substantially increase the mass loss of the implant matrix and lead to a growing pore network. The diffusive transport of the drug, polymer, and ionized species can face some sort of obstruction due to the pore structure. Therefore, quantifying the time evolution of the solid fraction, or porosity, of the implant and average pore size is important, as it affects the diffusion rates of the drug, polymers, and ionized species. Accordingly, we derived the following equation to determine the dynamic porosity of the implant during the degradation, erosion, release, and dissolution processes (eq 20):

$$\varepsilon_{SF}(t) = 1 - \frac{L_{im}}{V_{im}}\int_{R_{im}}^{R(t)}\left(\left[\sum_{i=1}^{i=2}\frac{1}{\rho_i}\sum_{k=J_{i,min}}^{L_p}p_{i,k}(t,r) + \frac{1}{\rho_d}(\xi(t,r) + m(t,r))\right]2\pi r \cdot dr\right) \tag{20}$$

where ρ_d and ρ_i are the skeletal densities of the drug and polymer, respectively. The $\varepsilon_{SF}(t)$ value is used in the following equations to calculate the time evolution of the average pore radius and surface area of the pores (eqs 21 and 22):

$$R_p(t) = \sqrt{\frac{\varepsilon_{SF}(t)V_{im}}{2n\pi R_{im}}} \tag{21}$$

$$SA_p(t,r) = 2\pi n R_p(t)dr \tag{22}$$

where V_{im} is the volume of the implant and n is the number of pores in the implant (assumed to remain unchanged and calculated by solving the eq 21 for n, using the initial values of the average pore radius and porosity: $n = (\varepsilon_{SF_0}V_{im})/(2\pi R_{p_0}^2 R_{im})$).

The pore diffusion theory was originally described by Ferry[50] and is used to model the hindered transport of molecules through liquid-filled pores, and it is used to obtain the obstruction coefficients for a diffusing species i (eq 23):

$$\omega_{i,m}(t) = \varepsilon_{SF}(t)\left(1 - \frac{Mr_i}{R_p(t)}\right)^2 \tag{23}$$

where Mr_i is the molecular radius of the diffusing molecules—drug, polymer molecules, or H^+ ions.

2.1.7. Initial Conditions. The initial conditions are presented in the Supporting Information.

2.1.8. Numerical Implementation. The above system of partial differential equations—described by eqs 7 and 12−19—is solved numerically using the method of lines; every space derivative is approximated according to the method of lines, leading to a set of ordinary differential equations (ODEs). This compartmental approach allows us to use the ODE solvers implemented in Simcyp physiologically based pharmacokinetic (PBPK) Simulator Version 23. The rest of the equations are solved analytically at each time step. The list of all primary input model parameters and state variables, along with their symbols and units, are listed in Tables 1 and 2.

Table 1. List of Model State Variables

state variable	symbol	units
radius of the wetted region edge	R	m
nondissolved polymers masses	$p_{i,j}$	g
dissolved polymers masses	$q_{i,j}$	g
trapped solid drug mass	ξ	g
untrapped solid drug mass	m	g
dissolved drug concentration in implant	C	g/m^3
dissolution media drug concentration	C_{if}	g/m^3
H^+ ion concentration in implant	$[H^+]$	M[a]
H_{if}^+ ion concentration in dissolution media	$[H_{if}^+]$	M[a]
H^+ ion amount in implant	H^+	mol
H_{if}^+ ion amount in dissolution media	H_{if}^+	mol

[a]M is mol/L.

2.2. Model Validation. The primary objectives for the selection of a compound-formulation validation set were: (a) to robustly challenge the model by picking complex and varied formulations, and (b) to demonstrate the predictive capability of the model. Moreover, it was important to us that sufficient *in vitro* characterization of the implant had been performed (LA/GA ratio, MW, polymer mass, *etc.*) and was available in the literature to allow simulation of the formulation's behavior without the need for speculation or fitting of these essential parameters. In line with these criteria, we have chosen to evaluate the model's performance against different solid long-acting implants comprising four compounds: namely, buserelin, afamelanotide, brimonidine, and nafarelin.

The following four case studies show tables in the Supporting Information with values of the parameters used in the model. The source of their value is referenced in the "Reference" column. For the sake of understanding, "Predicted" means the value is directly computed analytically based on the value of other inputs, using well-known formulas, while the entry "Optimized" means that the value has

https://doi.org/10.1021/acsabm.4c01054
ACS Appl. Bio Mater. XXXX, XXX, XXX−XXX

Table 2. List of Primary Model Parameters Summarized, Excluding Parameters Function of Those

parameter	symbol	units
viscosity of dissolution media	μ	mPa·h
radius of the implant	R_{im}	m
surface tension of dissolution media	Γ	$g{\cdot}h^{-2}$
average implant pore radius	R_p	m
contact angle/implant hydrophobicity	Θ	radian
permeation scalar	D_w	
volumetric porosity of the implant	ε_{SF}	
length of the implant	L_{im}	m
volume of the implant	V_{im}	m^3
volume of the dissolution media	V_{if}	m^3
initial mass of the implant	M_{im}	g
molar ratio of PLA polymers in the polymer mixture	Ψ	
hydrolysis rate constant of PLGA bonds	$K_{hyd,i}$	$M^{-1}{\cdot}h^{-1}$
minimum chain length of undissolved polymers	$J_{i,min}$	
molecular radius of polymer	Mr_q	m
molecular radius of H^+ ions	Mr_{H^+}	m
molecular radius of the drug	Mr_c	m
diffusivity of dissolved polymers in dissolution media	$D_{q,if}$	$m^2{\cdot}h^{-1}$
diffusivity of the drug in dissolution media	$D_{c,if}$	$m^2{\cdot}h^{-1}$
diffusivity of H^+ ions	$D_{H^+,if}$	$m^2{\cdot}h^{-1}$
aqueous solubility of the drug	C_s	$g{\cdot}m^{-3}$
diffusion layer thickness	h_{DLM}	m
ionization proportionality constant of polymer	k_{p^+}	
deionization constant rate of polymer	k_{p^-}	$M^{-1}{\cdot}h^{-1}$
polymer skeletal density	ρ_i	$g{\cdot}m^{-3}$
drug particle skeletal density	ρ_d	$g{\cdot}m^{-3}$
initial releasable fraction of drug	RF	
dose of drug in the implant at initial time	dose	g
initial pH of the dissolution media	pH_0	
weights of Gaussian component of initial PLGA mol. weights	$W_{[k]}$	
molecular weight of LA/GA monomers	$Mw_{M,i}$	Da
mean of Gaussian components of initial PLGA mol. weights	$Mw_{[k]}$	Da
SD of Gaussian components of initial PLGA mol. weights	$\sigma_{Mw,[k]}$	Da

been determined numerically so that the output can match the published release data.

2.2.1. Buserelin. Buserelin is a synthetic peptide, the analogue of the natural gonadotropin-releasing hormone (GnRH/LH-RH), and it is used for the treatment of hormone-responsive cancers such as carcinoma of the prostate gland in males and endometriosis in females. Subcutaneous implants of buserelin are commercially available under the brand names Suprefact Depot 2 Months and Suprefact Depot 3 Months. The physicochemical properties of buserelin, such as log P and pK_a, were obtained from DrugBank. An *in vitro* release study of the commercial buserelin implant was reported in the literature.[51] The implant-related information such as dimensions and drug loading, and relevant information about the experimental conditions were extracted from Schliecker et al.[51] and a product monograph on the commercial implant. All of the input parameters for the simulation, along with their references, are listed in Table S1.

The mean and error bounds calculated from six replicates were digitized from Figure 2 of Schliecker et al.'s publication.[51] The model was optimized by fitting to the release profile of the buserelin implant, with ionization proportionality constant, deionization constant, initial releasable fraction, and initial porosity estimated. A sensitivity study was conducted to demonstrate the effect on the predicted release profile of varying key CQAs, specifically the mean and standard deviation of the polymer MW, the GA/LA ratio, volumetric porosity, and mean pore size.

2.2.2. Afamelanotide. Afamelanotide is a synthetic peptide, the analogue of α-melanocyte stimulating hormone, and indicated to prevent phototoxicity in adult patients with erythropoietic protoporphyria. Subcutaneous implants of afamelanotide under the brand name SCENESSE were approved by the FDA in 2019. The physicochemical properties of Afamelanotide such as log P and pK_a were obtained from the DrugBank. An *in vitro* release study using bespoke afamelanotide containing PLGA implants was reported in the literature.[52,53] The implant-related information such as dimensions and drug loading, and relevant information about the experimental conditions were extracted from Bhardwaj and Blanchard's publication[53] for the manufactured implants using PLGA with lactide-to-glycolide molar ratios of 0.5 but different molecular weights, which were reported in terms of inherent viscosity (dL/g). The data from the 0.2 and 0.6 dL/g implants were utilized in the model validation. The PLGA manufacturer Evonik provided the mean molecular weight of PLGA products corresponding to these respective inherent viscosities (although it was not possible to unambiguously identify the products since both acid and ester end-capped PLGA products corresponded to these inherent viscosities). All of the input parameters for the simulation, along with their references, are listed in Table S2.

Data corresponding to the 0.2 and 0.6 dL/g implants (mean values from three replicates) were digitized (Engauge digitizer 12.1) from Figure 1 of Bhardwaj and Blanchard's publication.[53] The model was initially optimized by fitting to the release profile of the afamelanotide implant with PLGA inherent viscosity of 0.6 dL/g, with ionization proportionality constant, deionization constant, initial releasable fraction, and initial porosity estimated. Predictions of the release of the 0.2 dL/g implant were subsequently made, accounting for the different properties of the polymer. The ionization proportionality constant was optimized by fitting to the 0.2 dL/g release profile (we inferred that the end-capping differed in the 0.2 and 0.6 dL/g polymers and were unable to recover the release profile of the data without making this change).

2.2.3. Brimonidine. Brimonidine is an adrenergic agonist used for the management of Glaucoma. It decreases intraocular pressure by reducing aqueous humor production and increasing uveoscleral outflow.[54,55] The drug's physicochemical properties such as log P and pK_a were obtained from experimental data reported in the literature.[56] The intrinsic solubility of brimonidine was calculated by using the solubility module in SIVA 4.0.35.0. A US patent (Patent No. US20210113458A1) reported an *in vitro* release study involving PLGA implants of brimonidine, alongside details of the implant-related information such as dimensions, polymers used, drug loading, *etc.*[57] This data was used for the parameterization of the model. The data from three implants (EX1, EX3, EX4), which differed in the lactide-to-glycolide molar ratios (0.5, 0.75, and 0.875) and mean molecular weight (between 12,000 and 14,000 Da) were recorded. The list of all parameters and their sources for parametrizing the model are listed in Table S3. Data corresponding to the EX1, EX3, and EX4 formulations (mean values from four replicates at each formulation) were digitized from Figure 2 of US20210113458A1.[57] The model was initially optimized by fitting to the release profile of the EX1 implant, with ionization proportionality constant, deionization constant, initial releasable fraction, and initial porosity estimated. Predictions of the EX3 and EX4 profiles, accounting only for the different properties of the polymers used, were subsequently made.

2.2.4. Nafarelin. Nafarelin is a synthetic GnRH (gonadotropin-releasing hormone) analogue that is used medically as a hormonal treatment. It works by increasing or decreasing the production of certain hormones in the body, particularly the gonadotropins luteinizing hormone (LH) and follicle-stimulating hormone (FSH). The physicochemical properties of nafarelin, such as log P and pK_a, were obtained from DrugBank. An *in vitro* release study using bespoke nafarelin containing PLGA implants was reported by Sanders et al.[58] The implant-related information such as dimensions and drug loading, and relevant information about the experimental conditions for the manufactured implants using PLGA polymers with lactide-to-glycolide molar ratios of 80:20, 85:15, 90:10, 95:5 and 100:0 respectively, was extracted from the same publication. The molecular weights of the

https://doi.org/10.1021/acsabm.4c01054
ACS Appl. Bio Mater. XXXX, XXX, XXX−XXX

polymers used in experiments were not reported; however, a range of inherent viscosities (dL/g) between 0.33 and 0.38 dL/g were reported. The inherent viscosity is indicative of the molecular weight; however, this measurement is influenced by the solvent and other experimental variables. The molecular weights of these five polymers were therefore estimated based on available information. All of the input parameters for the simulation, along with their references, are listed in Table S4.

The cumulative release data from these formulations were digitized from Figure 5 of the Sanders et al.'s[58] paper. The model was initially optimized by fitting to the release profile of the 80:20 implant, with ionization proportionality constant, deionization constant, and initial releasable fraction optimized. Predictions of the release profile of the other four implants were subsequently made, accounting for the different properties of the polymers.

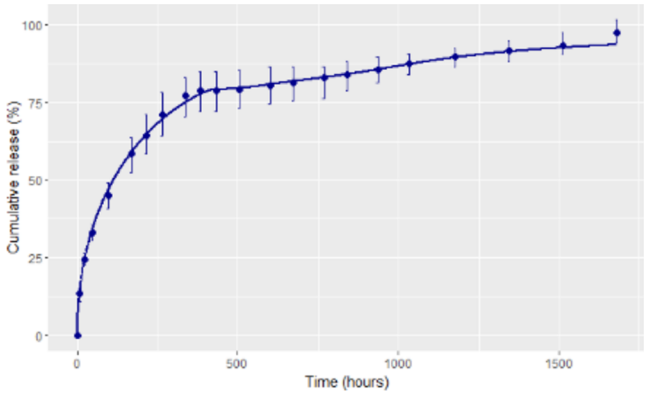

Figure 5. Observed and simulated *in vitro* cumulative release profile for the buserelin implant.

3. RESULTS

3.1. Buserelin. A simulation of the release profile based on the parameters listed in Table S1 is shown in Figure 5 alongside the observed data;[51] the mean and range from the replicates of the implant are shown in this example. As shown in Figure 5, the comparison indicates that the observed data are in close agreement with the simulated release. The simulated-to-observed ratio as a function of time was plotted and is shown in Figure S1.

Results from a sensitivity analysis are also shown for this case study, with the effect of a 10% decrease/increase in the baseline parameter value from Table S1 on the release profile shown for the GA/LA ratio, immediate release fraction, mean and standard deviation of the polymer MW, volumetric porosity, and mean pore size shown in panels a–f of Figure 6.

The results from sensitivity analysis based on this case study demonstrate that the model's behavior is reasonable. A higher lactide-to-glycolide ratio in the PLGA composition makes the implant more hydrophobic, hence, delaying the water penetration within the implant and its hydrolysis and drug

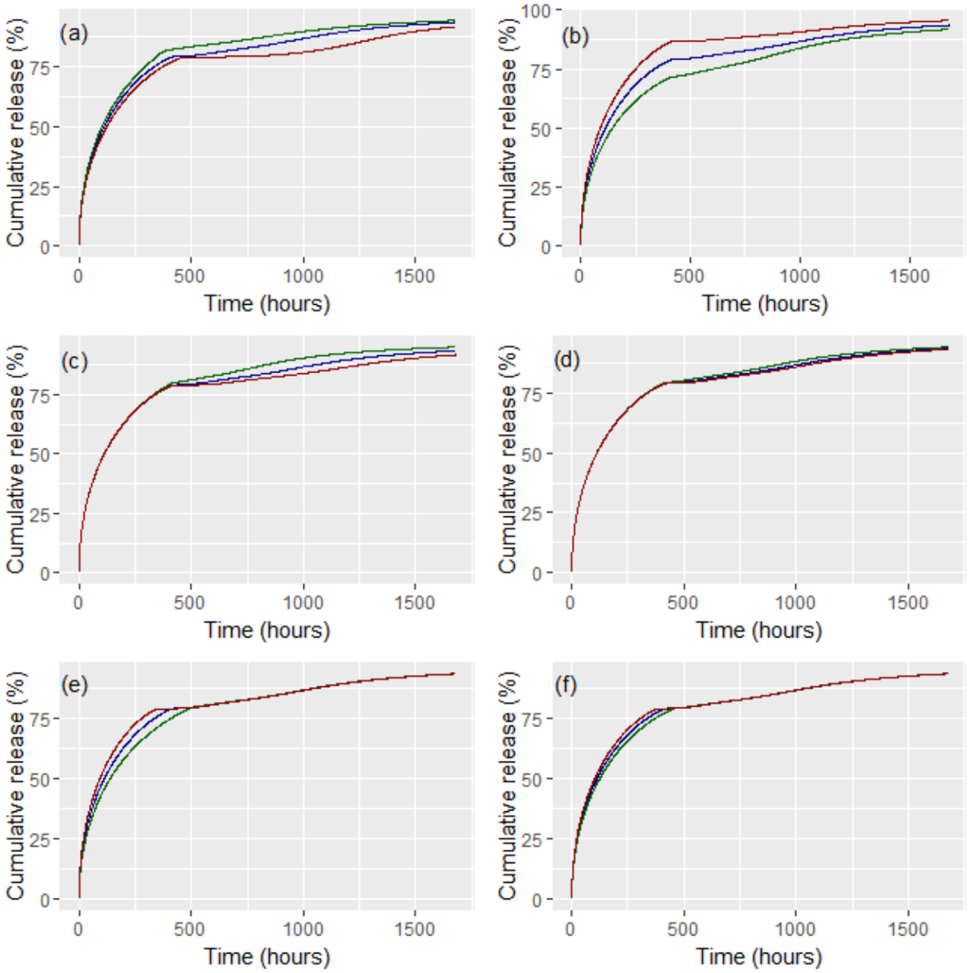

Figure 6. Results from local sensitivity analysis for the buserelin case study, demonstrating the effects of a plus/minus 10% change in (a) GA/LA molar ratio; (b) initial release fraction; (c) mean MW of polymer; (d) SD MW of polymer; (e) fractional volumetric porosity; and (f) mean pore size.

https://doi.org/10.1021/acsabm.4c01054
ACS Appl. Bio Mater. XXXX, XXX, XXX–XXX

release (Figure 6a). A larger immediate release fraction speeds up release in the initial phase (Figure 6b). As the PLGA molecular weight increases, the number of hydrolytically accessible bonds also increases, and due to the increased molecular entanglement and cross-linking, it makes the implant more resistant to degradation, therefore reducing the drug release rate (Figure 6c). Greater variability in the polymer molecular weight slows the release (Figure 6d). A larger volumetric porosity and a larger mean pore size increase the release rate (Figure 6e,f). The effects of parameter variations on the release profile are sensitive to the baseline parameters and the magnitude of parameter changes; however, the direction of effect is representative of the model sensitivities.

3.2. Afamelanotide. Simulations of the release profiles based on the parameters listed in Table S2 are shown in Figure 7

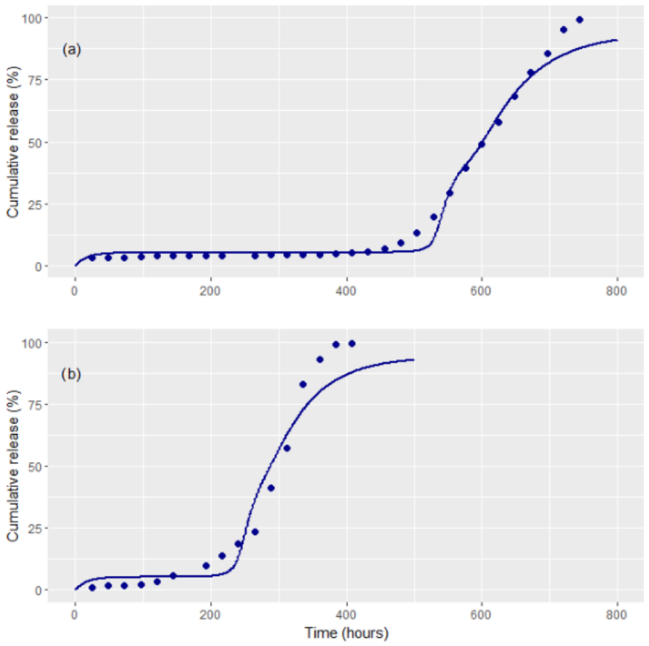

Figure 7. Observed and simulated *in vitro* cumulative release profile for the two afamelanotide implants: (a) 0.6 dL/g; (b) 0.2 dL/g.

alongside the observed data;[53] the points represent the mean values taken over the replicates. The data from the 0.6 dL/g implant were used for model calibration, and the release profile was well captured. The profile following extrapolation to the 0.2 dL/g implant was also well captured (with only an adjustment made to the ionization proportionality constant). The difference in the release profiles can be primarily attributed to a large difference in the molecular weight of the PLGA. The simulated-to-observed ratio *vs* time for all of the observations is presented in Figure S2.

3.3. Brimonidine. Simulations of the release profiles based on the parameters listed in Table S3 are shown in Figure 8 alongside the observed data;[57] the data points represent mean values taken over the replicates. The data from the EX1 implant were used in model calibration, and the release profile was well captured. The profiles of the EX3 and EX4 implants required extrapolations with the only adjustments being made to the CQAs of the implants. The simulated-to-observed ratio *vs* time profile is shown in Figure S3. These release profiles were also reasonably well captured. The difference in the release profiles can be primarily attributed to the difference in the lactide-to-

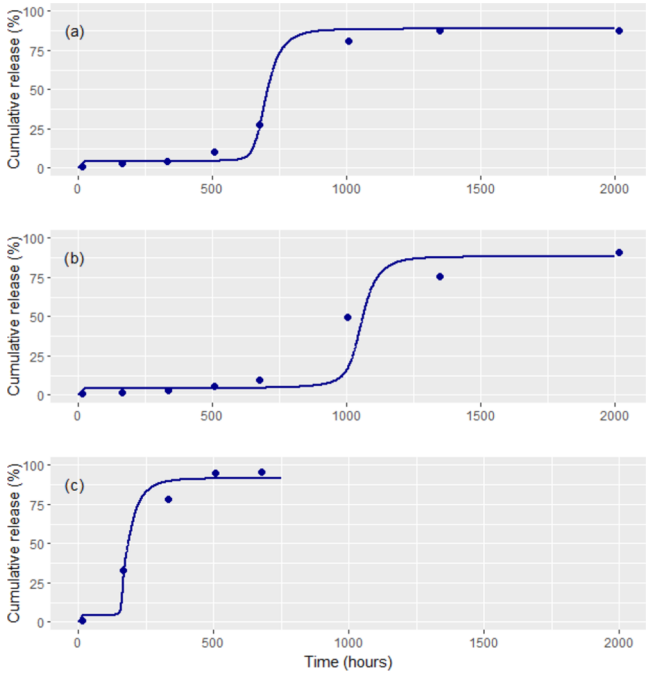

Figure 8. Observed and simulated *in vitro* cumulative release profile for the three brimonidine implants: (a) EX1; (b) EX3; and (c) EX4.

glycolide molar ratio of the implants; however, there were also differences in the end-capping between the experiments.

3.4. Nafarelin. Simulations of the release profiles based on the parameters listed in Table S4 are shown in Figure 9 alongside the observed data:[58] the points represent mean values taken over the replicates. The model was initially optimized by fitting to the release profile of the 80:20 implant, with extrapolations to the other four implants subsequently made: only differences in the CQAs of the implants were accounted for extrapolations. The simulated profile for the 80:20 implant was well captured. The successively later onsets of the tertiary phase of release in the 90:10, 95:5, and 100:0 implants were predicted; however, for this case study, the experimental data indicated an earlier onset and a slower release rate relative to simulations. The simulated-to-observed ratios *vs* time plots are presented in Figure S4 for five different formulations.

4. DISCUSSION

We noted in the introduction that PLGA-based formulations were first approved for clinical use in 1989; however, in the subsequent 35-year period, relatively few PLGA-based products in the form of solid implants, microspheres, or in situ forming gels have been approved. Further, despite the FDA commencing a regulatory science program to support the development of generic products in 2013, with a research focus on analytical tools for the characterization of PLGA polymers, impacts of PLGA characteristics and manufacturing conditions on product performance, *in vitro* drug release testing and *in vitro-in vivo* correlations (IVIVCs) of PLGA-based products, and modeling tools to facilitate formulation design and bioequivalence studies of PLGA-based drugs, the generic products following a decade of collaborative research by the FDA, academia and industry, were only approved by the FDA in 2023.

The sustained release that may be achieved by PLGA-based formulations helps to reduce dosing frequency, maintain stable concentrations of API, and may improve patient compliance.[59]

https://doi.org/10.1021/acsabm.4c01054
ACS Appl. Bio Mater. XXXX, XXX, XXX−XXX

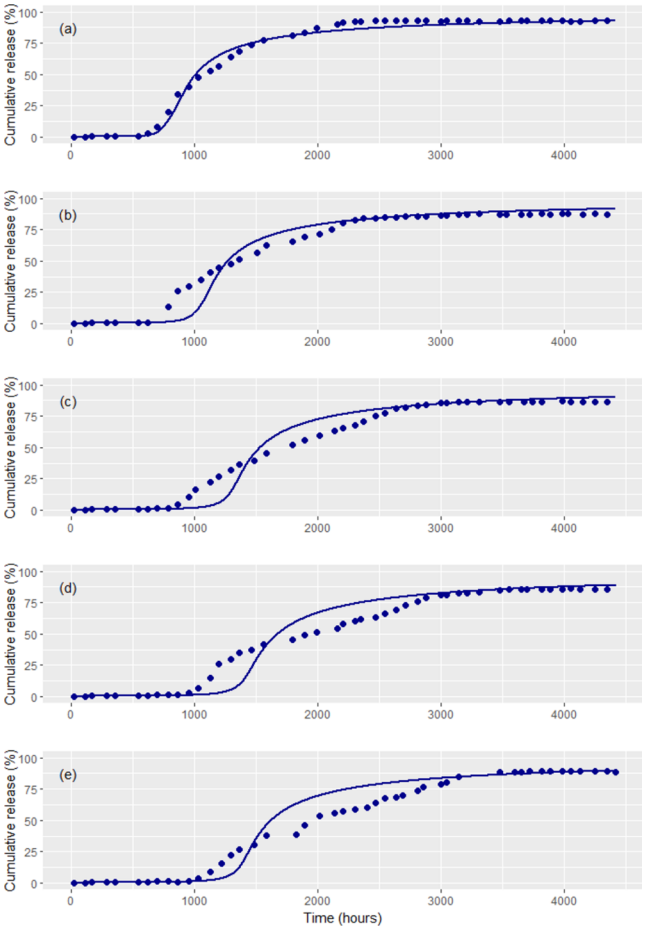

Figure 9. Observed and simulated *in vitro* cumulative release profile for the five nafarelin implants: (a) 80:20; (b) 85:15; (c) 90:10; (d) 95:5; and (e) 100:0.

The biodegradable nature of PLGA compared with other polymers such as ethylene vinyl acetate (EVA) is an undoubted advantage; however, the complex interplay between the physicochemical properties of the polymer, the API, and the drug delivery system has been a particular barrier in the development of generic products. Wang et al.[59] noted that even when candidate generic products qualitatively (Q1) and quantitatively (Q2) match reference-listed drug products in terms of inactive ingredients—so-called Q1/Q2 compliance—is insufficient to ensure bioequivalence between test and reference products.[59] The Q1/Q2 requirement does not capture other parameters, such as the manufacturing process, drug distribution within the PLGA product, and drug crystallinity.[60]

To further advance the regulatory science of PLGA-based LAIs, there is an immediate need to understand the critical formulation parameters that may affect product performance *in vitro* and *in vivo*. Mathematical models of polymer degradation and subsequent drug release offer a unique opportunity to understand how the physicochemical properties of drug molecules/polymer, implant-specific properties, critical formulation attributes, and the test environment influence the *in vitro* release mechanisms of LAI drug products and their disposition characteristics.[61]

The release of drugs from PLGA-based implants is influenced by intrinsic and extrinsic factors. These factors include qualitative (Q1) and quantitative (Q2) compositions, microstructural characteristics, and release conditions. The intrinsic factors will have a direct influence on the drug release; for example, a high molecular weight polymer within the implant is expected to slow down the drug release compared to the lower molecular polymer under similar testing conditions. On the contrary, the extrinsic factors such as release temperature and composition of release media, for example, the presence of surfactants and concentration of surfactants, influence the dynamics of the process, thereby changing the rate processes such as rate of fluid penetration into the implant, degradation rate of polymer, *etc.*, for the same implant under different testing conditions.[62]

The mathematical model described in this work, as implemented in the V23 release of the Simcyp Simulator, takes as input the geometry of the prepared implant, information on the CQAs of the PLGA and implant itself, and a system of equations that describe the degradation of the PLGA and subsequent release of drug. The key processes in the model include water influx into the porous structure of the implant, initial hydrolysis followed by autocatalytic hydrolysis, dissolution of oligomer and monomer into the dissolution media accompanied by mass loss and a growing pore network, liberation, dissolution, and diffusion of the trapped drug. As output, the model can simulate the cumulative release of the drug in the solvent with further profiles that characterize the penetration of fluid into the implant (percent water occupation), pH, the molecular weight of PLGA, volumetric porosity, and mass of PLGA (and LA and GA, respectively). A weight of information on the degradation of the implant that would be time-consuming, expensive, or unavailable from other sources allows new insights into the degradation of the implant over and above the raw data from *in vitro* release experiments that are used to tune the model parameters. All of the implants studied in this article were reported to be manufactured using the extrusion process, except for Buserelin, which was manufactured using the compression molding technique. However, there is no detailed information about the exact manufacturing conditions, and manufacturing process variables are likely different, in addition to testing them under different test conditions; thus, it was necessary to tune the model first for some of the *in vitro* release data before studying the changing CQAs or characteristics of the *in vitro* test environment.

The input requirements for the mathematical model are substantial since information on the API, polymers, and the implant microstructure are required. The necessary information to parametrize the model may be almost entirely obtained from public databases, polymer product sheets, and high-quality *in vitro* studies,[63] which characterize the microstructure of the manufactured implant before commencing experiments. However, even in cases where near complete information is available, a small number of parameters (principally the ionization proportionality constant and immediate release fraction) needed estimation using data from a controlled release experiment; our work suggests a sharp optimum (a sudden improvement in the fitting during parameter estimation) is found when few parameters need to be estimated. In the case studies reported in this work, a wider pool of parameters was estimated since there was insufficient information available in the source publications to fully parametrize the model. In principle, this raises a problem associated with overfitting; however, our numerical work suggests that rather than additional free parameters allowing a significant improvement in the fit to *in vitro* data, we instead found that there was a significant uncertainty associated with the values of the

https://doi.org/10.1021/acsabm.4c01054
ACS Appl. Bio Mater. XXXX, XXX, XXX−XXX

estimated model parameters; known values for properties such as mean pore size and volumetric porosity would simply reduce this uncertainty rather than compromise the quality of fit to in vitro data. Following calibration using one data set, the extrapolations made within the case studies suggest the model extrapolated reliably with release profiles responding to changes in parameters in a physically plausible manner. The observed differences between the simulated release profiles and observations for the brimonidine and nafarelin case studies may be attributed to the microstructural changes that might also be affected by the material changes. However, for the sake of simplicity for running the simulations, we assumed that the implant parameters are constant for different polymer implants of the same drug. Also, it is important to note that the structure of the implant throughout the release experiment tends to be influenced by the erosion pattern, *i.e.*, bulk *vs* surface, and a shift in the release mechanisms may be possible because of a process or material change, or both, which we have not accounted for during the development of case studies due to the lack of thorough characterization information. This, we plan to investigate in our future studies, thereby addressing the discrepancies between the simulation data *vs* observed data. If necessary, we would account for additional mechanisms and processes to accurately describe the observed data.

The adjusted parameters for the cases discussed in this paper, namely, polymer ionization proportionality constant and deionization constants, impact the H^+ ions mass in the implant, thereby impacting the polymer degradation and subsequently liberation, dissolution, and diffusion of the active from inside to the outside of the implant. Another model parameter, "initial releasable fraction" in the model, is a fraction of the total amount of dose within the implant that is present in the pores. However, these pores are distributed spatially within the implant at the surface or within the implant. Further, due to the slow wetting process in the case of a solid implant, only surface pores are expected to be in contact with the release media during the initial hours; thus, the drug released from these surface pores is seen as burst in release experiments.

Other parameters such as the critical chain length of the oligomer directly influence the polymer mass loss from the implant and indirectly influence H^+ ion mass in the implant, thereby modulating the drug release from the implant. Again, it may be possible that for some of the parameter combinations, one or more parameters in the model can be less sensitive, and to understand the parameter impact, it may be necessary to look at the profiles other than drug release, for example, polymer degradation, water occupation, *etc.*

Additionally, while the focus of this work has been on documenting and validating the mathematical model for polymer degradation and drug release in the in vitro setting, the model can be used in conjunction with PBPK modeling for the human *in vivo* setting; this requires a release into the local injection site, rather than a solvent, and accounting for the local cell drug partition from interstitial fluid and systemic drug transfer, which are governed by the physicochemical properties of the drug molecule. Finally, future work may focus on improving the model's ability to predict the drug release by accounting for additional processes and/or assumptions related to the polymer degradation and diffusion and adding features to the models, for example, the ability to input the pore size distribution data for an implant, and outputting of pore size distribution as a function of time for data analysis.

5. CONCLUSIONS

A predictive, comprehensive, bottom-up mechanistic model was developed to predict the *in vitro* drug release from PLGA-based solid implant formulations. The model takes into account all of the following kinetic rate processes that take place for the drug to be released from the formulation: (1) water/dissolution media influx into the porous structure of the implant, (2) initial noncatalytic hydrolysis of PLGA, (3) autocatalytic hydrolysis phase (4) substantial mass loss of the polymer due to dissolution of small oligomers and monomers into the aqueous medium, (5) liberation of the trapped solid drug from the polymer matrix, (6) dissolution of solid drug into the wetted pore network, (7) diffusion of the dissolved drug out of the implant, and (8) accumulation of the dissolved drug in the dissolution media. The developed model has been validated by the *in vitro* release data obtained from subcutaneous/intravitreal implants with four different compounds, including buserelin, afamelanotide, brimonidine, and nafarelin.

In conclusion, the developed model has proven to be a valuable tool for predicting and understanding drug release behavior from PLGA solid implants. Through the use of the model, it has been possible to study the complex interactions between the polymer and the drug, as well as to evaluate the impact of all CQAs for PLGA-based formulation such as molecular weight, lactide-to-glycolide molar ratio, and hydrophobicity on drug release. The model has provided valuable insights into the kinetics and mechanism of drug release from PLGA solid implants and has demonstrated the potential for optimizing the design of these systems for specific medical applications. The *in vitro* release model coupled with a PBPK modeling framework gives a more complete picture of the drug's behavior in the body, which can provide valuable information to support bioequivalence study in a drug development program. The focus of future work will be on enhancing the model predictions for drug release; additionally, we acknowledge the fact that there is likely scope for the demonstration of additional cases for validation of the model, which we plan to take up as a future activity.

■ ASSOCIATED CONTENT

Supporting Information

The Supporting Information is available free of charge at https://pubs.acs.org/doi/10.1021/acsabm.4c01054.

Initial conditions for the equations, model parametrization tables (Tables S1−S4), and fold error *vs* time plots (Figures S1−S4) (PDF)

■ AUTHOR INFORMATION

Corresponding Authors

Naresh Mittapelly − *Certara Predictive Technologies (CPT), Simcyp Division, Sheffield S1 2BJ, U.K.*; orcid.org/0000-0003-0130-4519; Email: naresh.mittapelly@certara.com

Frederic Y. Bois − *Certara Predictive Technologies (CPT), Simcyp Division, Sheffield S1 2BJ, U.K.*; orcid.org/0000-0002-4154-0391; Email: frederic.bois@certara.com

Authors

Alexandre Djehizian − *Certara Predictive Technologies (CPT), Simcyp Division, Sheffield S1 2BJ, U.K.*

Krishna Chaitanya Telaprolu − *Certara Predictive Technologies (CPT), Simcyp Division, Sheffield S1 2BJ, U.K.*

https://doi.org/10.1021/acsabm.4c01054
ACS Appl. Bio Mater. XXXX, XXX, XXX−XXX

Kevin McNally − *Certara Predictive Technologies (CPT), Simcyp Division, Sheffield S1 2BJ, U.K.*
Santosh Kumar Puttrevu − *Certara Predictive Technologies (CPT), Simcyp Division, Sheffield S1 2BJ, U.K.*
Omid Arjmandi-Tash − *Certara Predictive Technologies (CPT), Simcyp Division, Sheffield S1 2BJ, U.K.*
Sebastian Polak − *Certara Predictive Technologies (CPT), Simcyp Division, Sheffield S1 2BJ, U.K.; Department of Pharmaceutical Technology and Biopharmaceutics, Faculty of Pharmacy, Jagiellonian University Medical College, 30-688 Krakow, Poland*

Complete contact information is available at: https://pubs.acs.org/10.1021/acsabm.4c01054

Author Contributions

All authors contributed to the manuscript, and they have all approved its final version. In addition, N.M. contributed to methodology, investigation, formal analysis, and data curation; A.D. contributed to methodology, investigation, and implementation; K.C.T. worked on formal analysis and data curation; K.M. contributed to formal analysis; S.K.P. worked on formal analysis and data curation; O.A.T. contributed to conceptualization and implementation; S.P. worked on methodology; and F.B. contributed to conceptualization and supervision.

Notes

The authors declare the following competing financial interest(s): All the authors are Certara UK Limited (Certara Predictive Technologies) employees.

■ ACKNOWLEDGMENTS

The authors acknowledge the assistance of Whitney Moro from Evonik Corporation, who assisted in making estimates of molecular weights of PLGA polymers. The authors also thank Natalie Morris, an employee of Certara U.K. Ltd., for her assistance with graphics design using Inkscape software.

■ ADDITIONAL NOTE

[1]This assumes that even when large nondissolved polymer molecules are degraded into still nondissolved polymer molecules, some drug will be released from the polymer matrix.

■ REFERENCES

(1) Takada, N.; Kawabe, H. *Drug Discovery in Japan: Investigating the Sources of Innovation*; Nagaoka, S., Ed.; Springer: Singapore, 2019.
(2) Lim, Y. W.; Tan, W. S.; Ho, K. L.; Mariatulqabtiah, A. R.; Abu Kasim, N. H.; Abd Rahman, N.; Wong, T. W.; Chee, C. F. Challenges and Complications of Poly(lactic-co-glycolic acid)-Based Long-Acting Drug Product Development. *Pharmaceutics* **2022**, *14* (3), No. 614, DOI: 10.3390/pharmaceutics14030614.
(3) D'Souza, S. S.; Selmin, F.; Murty, S. B.; Qiu, W.; Thanoo, B.; DeLuca, P. P. Assessment of fertility in male rats after extended chemical castration with a GnRH antagonist. *AAPS PharmSci* **2004**, *6* (1), 94−99.
(4) Gu, H.; Song, C.; Long, D.; Mei, L.; Sun, H. Controlled release of recombinant human nerve growth factor (rhNGF) from poly [(lactic acid)-co-(glycolic acid)] microspheres for the treatment of neurodegenerative disorders. *Polym. Int.* **2007**, *56* (10), 1272−1280.
(5) Mo, Y.; Lim, L.-Y. Paclitaxel-loaded PLGA nanoparticles: potentiation of anticancer activity by surface conjugation with wheat germ agglutinin. *J. Controlled Release* **2005**, *108* (2−3), 244−262.
(6) Murata, N.; Takashima, Y.; Toyoshima, K.; Yamamoto, M.; Okada, H. Anti-tumor effects of anti-VEGF siRNA encapsulated with PLGA microspheres in mice. *J. Controlled Release* **2008**, *126* (3), 246−254.
(7) Patel, P.; Mundargi, R. C.; Babu, V. R.; Jain, D.; Rangaswamy, V.; Aminabhavi, T. M. Microencapsulation of doxycycline into poly (lactide-co-glycolide) by spray drying technique: Effect of polymer molecular weight on process parameters. *J. Appl. Polym. Sci.* **2008**, *108* (6), 4038−4046.
(8) Yen, S.-Y.; Sung, K.; Wang, J.-J.; Hu, O. Y.-P. Controlled release of nalbuphine propionate from biodegradable microspheres: in vitro and in vivo studies. *Int. J. Pharm.* **2001**, *220* (1−2), 91−99.
(9) Fredenberg, S.; Wahlgren, M.; Reslow, M.; Axelsson, A. The mechanisms of drug release in poly (lactic-co-glycolic acid)-based drug delivery systems—a review. *Int. J. Pharm.* **2011**, *415* (1−2), 34−52.
(10) Park, K.; Skidmore, S.; Hadar, J.; Garner, J.; Park, H.; Otte, A.; Soh, B. K.; Yoon, G.; Yu, D.; Yun, Y.; et al. Injectable, long-acting PLGA formulations: Analyzing PLGA and understanding microparticle formation. *J. Controlled Release* **2019**, *304*, 125−134.
(11) Bassand, C.; Benabed, L.; Verin, J.; Danede, F.; Lefol, L.; Willart, J.-F.; Siepmann, F.; Siepmann, J. Hot melt extruded PLGA implants loaded with ibuprofen: How heat exposure alters the physical drug state. *J. Drug Delivery Sci. Technol.* **2022**, *73*, No. 103432.
(12) Yun, Y. H.; Lee, B. K.; Park, K. Controlled Drug Delivery: Historical perspective for the next generation. *J. Controlled Release* **2015**, *219*, 2−7.
(13) Garner, J.; Skidmore, S.; Park, H.; Park, K.; Choi, S.; Wang, Y. Beyond Q1/Q2: the impact of manufacturing conditions and test methods on drug release from PLGA-based microparticle depot formulations. *J. Pharm. Sci.* **2018**, *107* (1), 353−361.
(14) Hu, F.; Qi, J.; Lu, Y.; He, H.; Wu, W. PLGA-based implants for sustained delivery of peptides/proteins: Current status, challenge and perspectives. *Chin. Chem. Lett.* **2023**, *34* (11), No. 108250.
(15) Yu, L. X.; Amidon, G.; Khan, M. A.; Hoag, S. W.; Polli, J.; Raju, G.; Woodcock, J. Understanding pharmaceutical quality by design. *AAPS J.* **2014**, *16* (4), 771−783.
(16) Versypt, A. N. F.; Pack, D. W.; Braatz, R. D. Mathematical modeling of drug delivery from autocatalytically degradable PLGA microspheres–a review. *J. Controlled Release* **2013**, *165* (1), 29−37.
(17) Antheunis, H.; van der Meer, J.-C.; de Geus, M.; Kingma, W.; Koning, C. E. Improved mathematical model for the hydrolytic degradation of aliphatic polyesters. *Macromolecules* **2009**, *42* (7), 2462−2471.
(18) Siparsky, G. L.; Voorhees, K. J.; Miao, F. Hydrolysis of polylactic acid (PLA) and polycaprolactone (PCL) in aqueous acetonitrile solutions: autocatalysis. *J. Polym. Environ.* **1998**, *6* (1), 31−41.
(19) Nishida, H.; Yamashita, M.; Nagashima, M.; Hattori, N.; Endo, T.; Tokiwa, Y. Theoretical prediction of molecular weight on autocatalytic random hydrolysis of aliphatic polyesters. *Macromolecules* **2000**, *33* (17), 6595−6601.
(20) Lyu, S.; Schley, J.; Loy, B.; Lind, D.; Hobot, C.; Sparer, R.; Untereker, D. Kinetics and time− temperature equivalence of polymer degradation. *Biomacromolecules* **2007**, *8* (7), 2301−2310.
(21) Antheunis, H.; van der Meer, J.-C.; de Geus, M.; Heise, A.; Koning, C. E. Autocatalytic equation describing the change in molecular weight during hydrolytic degradation of aliphatic polyesters. *Biomacromolecules* **2010**, *11* (4), 1118−1124.
(22) Batycky, R. P.; Hanes, J.; Langer, R.; Edwards, D. A. A theoretical model of erosion and macromolecular drug release from biodegrading microspheres. *J. Pharm. Sci.* **1997**, *86* (12), 1464−1477.
(23) Ding, A. G.; Shenderova, A.; Schwendeman, S. P. Prediction of microclimate pH in poly (lactic-co-glycolic acid) films. *J. Am. Chem. Soc.* **2006**, *128* (16), 5384−5390.
(24) Göpferich, A. Polymer bulk erosion. *Macromolecules* **1997**, *30* (9), 2598−2604.
(25) Chen, Y.; Zhou, S.; Li, Q. Mathematical modeling of degradation for bulk-erosive polymers: applications in tissue engineering scaffolds and drug delivery systems. *Acta Biomater.* **2011**, *7* (3), 1140−1149.
(26) Wang, Y.; Pan, J.; Han, X.; Sinka, C.; Ding, L. A phenomenological model for the degradation of biodegradable polymers. *Biomaterials* **2008**, *29* (23), 3393−3401.

(27) Charlier, A.; Leclerc, B.; Couarraze, G. Release of mifepristone from biodegradable matrices: experimental and theoretical evaluations. *Int. J. Pharm.* **2000**, *200* (1), 115−120.
(28) Faisant, N.; Siepmann, J.; Benoit, J.-P. PLGA-based microparticles: elucidation of mechanisms and a new, simple mathematical model quantifying drug release. *Eur. J. Pharm. Sci.* **2002**, *15* (4), 355−366.
(29) Berchane, N.; Carson, K.; Rice-Ficht, A.; Andrews, M. Effect of mean diameter and polydispersity of PLG microspheres on drug release: Experiment and theory. *Int. J. Pharm.* **2007**, *337* (1−2), 118−126.
(30) Raman, C.; Berkland, C.; Kim, K. K.; Pack, D. W. Modeling small-molecule release from PLG microspheres: effects of polymer degradation and nonuniform drug distribution. *J. Controlled Release* **2005**, *103* (1), 149−158.
(31) Thombre, A. G.; Himmelstein, K. A simultaneous transport-reaction model for controlled drug delivery from catalyzed bioerodible polymer matrices. *AIChE J.* **1985**, *31* (5), 759−766.
(32) Joshi, A.; Himmelstein, K. J. Dynamics of controlled release from bioerodible matrices. *J. Controlled Release* **1991**, *15* (2), 95−104.
(33) Siepmann, J.; Faisant, N.; Benoit, J.-P. A new mathematical model quantifying drug release from bioerodible microparticles using Monte Carlo simulations. *Pharm. Res.* **2002**, *19* (12), 1885−1893.
(34) Lemaire, V.; Belair, J.; Hildgen, P. Structural modeling of drug release from biodegradable porous matrices based on a combined diffusion/erosion process. *Int. J. Pharm.* **2003**, *258* (1−2), 95−107.
(35) Zhang, M.; Yang, Z.; Chow, L. L.; Wang, C. H. Simulation of drug release from biodegradable polymeric microspheres with bulk and surface erosions. *J. Pharm. Sci.* **2003**, *92* (10), 2040−2056.
(36) Prabhu, S.; Hossainy, S. Modeling of degradation and drug release from a biodegradable stent coating. *J. Biomed. Mater. Res., Part A* **2007**, *80A* (3), 732−741.
(37) Rothstein, S. N.; Federspiel, W. J.; Little, S. R. A simple model framework for the prediction of controlled release from bulk eroding polymer matrices. *J. Mater. Chem.* **2008**, *18* (16), 1873−1880.
(38) Rothstein, S. N.; Federspiel, W. J.; Little, S. R. A unified mathematical model for the prediction of controlled release from surface and bulk eroding polymer matrices. *Biomaterials* **2009**, *30* (8), 1657−1664.
(39) Zhao, A.; Hunter, S.; Rodgers, V. Theoretical prediction of induction period from transient pore evolvement in polyester-based microparticles. *J. Pharm. Sci.* **2010**, *99* (11), 4477−4487.
(40) Ford, A. N.; Pack, D. W.; Braatz, R. D. Multi-Scale Modeling of PLGA Microparticle Drug Delivery Systems. In *Computer Aided Chemical Engineering*; Elsevier, 2011; Vol. *29*, pp 1475−1479.
(41) Casalini, T.; Rossi, F.; Lazzari, S.; Perale, G.; Masi, M. Mathematical Modeling of PLGA Microparticles: From Polymer Degradation to Drug Release. *Mol. Pharmaceutics* **2014**, *11* (11), 4036−4048.
(42) Koursari, N.; Arjmandi-Tash, O.; Trybala, A.; Starov, V. M. Drying of Foam under Microgravity Conditions. *Microgravity Sci. Technol.* **2019**, *31* (5), 589−601.
(43) McCabe, W. L.; Smith, J. C.; Harriott, P. *Unit Operations of Chemical Engineering*; McGraw-Hill, 1993.
(44) Zhu, X.; Braatz, R. D. A mechanistic model for drug release in PLGA biodegradable stent coatings coupled with polymer degradation and erosion. *J. Biomed. Mater. Res., Part A* **2015**, *103* (7), 2269−2279.
(45) Busatto, C.; Pesoa, J.; Helbling, I.; Luna, J.; Estenoz, D. Heterogeneous hydrolytic degradation of poly(lactic-co-glycolic acid) microspheres: Mathematical modeling. *J. Appl. Polym. Sci.* **2017**, *134* (43), No. 45464.
(46) Wang, J.; Flanagan, D. R. General solution for diffusion-controlled dissolution of spherical particles. 1. Theory. *J. Pharm. Sci.* **1999**, *88* (7), 731−738.
(47) Noyes, A. A.; Whitney, W. R. The Rate of Solution of Solid Substances in Their Own Solutions. *J. Am. Chem. Soc.* **1897**, *19* (12), 930−934.
(48) Nernst, W. Theorie der Reaktionsgeschwindigkeit in Heterogenen Systemen. *Z. Phys. Chem.* **1904**, *47U* (1), 52−55.
(49) Brunner, E. Reaktionsgeschwindigkeit in Heterogenen Systemen. *Z. Phys. Chem.* **1904**, *47U* (1), 56−102.
(50) Ferry, J. D. Statistical Evaluation of Sieve Constants in Ultrafiltration. *J. Gen. Physiol.* **1936**, *20* (1), 95−104.
(51) Schliecker, G.; Schmidt, C.; Fuchs, S.; Ehinger, A.; Sandow, J.; Kissel, T. In vitro and in vivo correlation of buserelin release from biodegradable implants using statistical moment analysis. *J. Controlled Release* **2004**, *94* (1), 25−37.
(52) Bhardwaj, R.; Blanchard, J. In vitro characterization and in vivo release profile of a poly (d,l-lactide-co-glycolide)-based implant delivery system for the α-MSH analog, melanotan-I. *Int. J. Pharm.* **1998**, *170* (1), 109−117.
(53) Bhardwaj, R.; Blanchard, J. In vitro evaluation of Poly(d,l-lactide-co-glycolide) polymer-based implants containing the α-melanocyte stimulating hormone analog, Melanotan-I. *J. Controlled Release* **1997**, *45* (1), 49−55.
(54) Cantor, L. B. Brimonidine in the treatment of glaucoma and ocular hypertension. *Ther. Clin. Risk Manage.* **2006**, *2* (4), 337−346.
(55) Toris, C. B.; Gleason, M. L.; Camras, C. B.; Yablonski, M. E. Effects of brimonidine on aqueous humor dynamics in human eyes. *Arch. Ophthalmol.* **1995**, *113* (12), 1514−1517.
(56) Bhagav, P.; Deshpande, P.; Pandey, S.; Chandran, S. Development and validation of stability indicating UV spectrophotometric method for the estimation of brimonidine tartrate in pure form, formulations and preformulation studies. *Pharm. Lett.* **2010**, *2* (3), 106−122.
(57) Shiah, J.-G. C. P. Sustained Drug Delivery Implant. U.S. Patent. US0113458A1, 2021.
(58) Sanders, L.; Kell, B.; McRae, G.; Whitehead, G. Prolonged controlled-release of nafarelin, a luteinizing hormone-releasing hormone analogue, from biodegradable polymeric implants: influence of composition and molecular weight of polymer. *J. Pharm. Sci.* **1986**, *75* (4), 356−360.
(59) Wang, Y.; Qin, B.; Xia, G.; Choi, S. H. FDA's Poly (Lactic-Co-Glycolic Acid) Research Program and Regulatory Outcomes. *AAPS J.* **2021**, *23* (4), No. 92.
(60) Garner, J.; Skidmore, S.; Park, H.; Park, K.; Choi, S.; Wang, Y. Beyond Q1/Q2: The Impact of Manufacturing Conditions and Test Methods on Drug Release From PLGA-Based Microparticle Depot Formulations. *J. Pharm. Sci.* **2018**, *107* (1), 353−361.
(61) Giolando, P. A.; Hopkins, K.; Davis, B. F.; Vike, N.; Ahmadzadegan, A.; Ardekani, A. M.; Vlachos, P. P.; Rispoli, J. V.; Solorio, L.; Kinzer-Ursem, T. L. Mechanistic Computational Modeling of Implantable, Bioresorbable Drug Release Systems. *Adv. Mater.* **2023**, *35* (51), No. 2301698.
(62) Costello, M. A.; Liu, J.; Chen, B.; Wang, Y.; Qin, B.; Xu, X.; Li, Q.; Lynd, N. A.; Zhang, F. Drug release mechanisms of high-drug-load, melt-extruded dexamethasone intravitreal implants. *Eur. J. Pharm. Biopharm.* **2023**, *187*, 46−56.
(63) Costello, M. A.; Liu, J.; Wang, Y.; Qin, B.; Xu, X.; Li, Q.; Smith, W. C.; Lynd, N. A.; Zhang, F. Manufacturing dexamethasone intravitreal implants: Process control and critical quality attributes. *Int. J. Pharm.* **2023**, *647*, No. 123515.

https://doi.org/10.1021/acsabm.4c01054
ACS Appl. Bio Mater. XXXX, XXX, XXX−XXX